Imaging ahead of and around the bit in a desert environment: DrillCAM field trial with wireless geophones and top-drive sensor

Ali Aldawood[1], Emad Hemyari[1], Ilya Silvestrov[1], and Andrey Bakulin[1]

https://doi.org/10.1190/tle40050374.1

Abstract

Advanced seismic-while-drilling (SWD) technologies are being utilized to steer drilling operations and provide high-resolution subsurface images around and ahead of the bit. We present a case study of SWD imaging using a recently acquired field data set from a desert environment with a complex near surface. Data acquisition is performed with wireless geophones and top-drive sensors using continuous real-time recording. The drill-bit noise data are analyzed while continuously recording in real time by using a specialized workflow that combines elements of SWD and conventional vertical seismic profiling processing with controlled seismic sources. First, the workflow enhances the direct wavefield to retrieve accurate first-break picks for traveltime tomographic inversion along east–west- and north–south-striking walkaway lines. Then, it extracts and enhances upgoing reflection events, illuminating parts of the subsurface around and ahead of the bit. During the final step, these upgoing reflections are imaged using the inverted velocity model to reconstruct a migrated subsurface image around the well. As is the case for land surface seismic in the presence of a complex near surface, we observe a significant variation of data quality for the orthogonal receiver lines. As a result, each line provides a robust image of a different part of the subsurface. The east–west-striking line's migrated image delineates a major shallow reflector that serves as a marker for predicting the drilling depth of a deeper horizon. Likewise, migrating upgoing reflections from the north–south line accurately maps a deeper target horizon ahead of the bit. The obtained SWD images assist in setting the casing points accurately and provide a more precise ahead-of-the-bit depth for different horizons with significantly less uncertainty than surface seismic.

Introduction

Seismic while drilling (SWD) uses the drill bit's vibrations to illuminate the subsurface structure (Rector and Marion, 1991; Haldorsen et al., 1995; Miranda et al., 1996; Bertelli and di Cesare, 1999; Poletto and Miranda, 2004). These vibrations are recorded by surface sensors and processed to obtain a reverse vertical seismic profiling (RVSP) data set (Rector and Marion, 1991; Khaled et al., 1996; Miranda et al., 1996). Making seismic measurements while drilling enables various drilling decisions to be optimized and reduces uncertainty without interfering with the drilling operation. It also avoids the cost of conventional wireline measurements (Greenberg, 2008).

SWD technology is challenging due to the weak signal strength of the drill bit. Due to a limited channel count, the aperture is restricted, and processing schemes for enhancing the low signal-to-noise ratio (S/N) of SWD data sets are limited. Al-Muhaidib et al. (2018) and Bakulin et al. (2020) present the DrillCAM system, which attempts to overcome some of these limitations by increasing the channel count significantly, applying a more sophisticated processing workflow, and using higher-quality downhole pilots. The system consists of the following components:

1) Wireless receivers are centered around the well, with an acquisition geometry as shown in Figure 1, to record the seismic waves traveling from the drill bit (source) and passing through the formations.
2) A top-drive sensor records in real time the drill-bit signature that travels along the drill string.
3) A downhole sensor records a more robust version of the drill-bit signature near the source, but this is currently saved in memory and only available after drill-string retrieval (Poletto and Miranda, 2004; Mathiszik et al., 2011; Bakulin et al., 2020) for more accurate non-real-time processing.

Bakulin et al. (2020) summarize initial results from the first field trial. They demonstrate the feasibility of utilizing the acquired SWD data and top-drive pilot to obtain reliable check shots (time-depth curves) in real time and kinematic predictions of critical reflectors ahead of the bit. These applications were demonstrated using RVSP data with a single wireless receiver at a small offset. This study utilizes almost the entire data set, composed of 2500 receivers, for SWD VSP processing and imaging of data from two orthogonal receiver line directions. The SWD system aims to obtain borehole geophysics deliverables such as

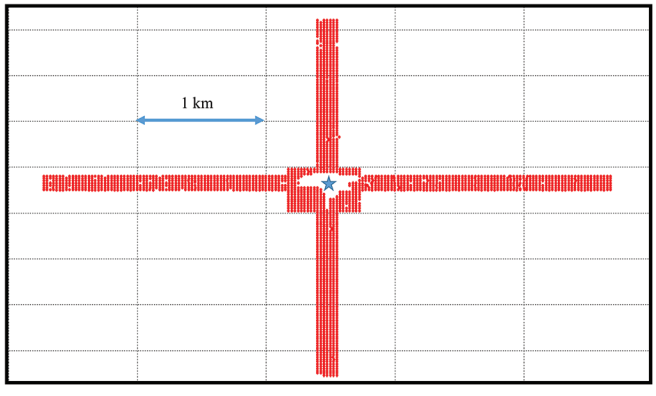

Figure 1. Acquisition geometry from the first DrillCAM field trial in the desert environment. A total of 2500 wireless receivers (single sensors) marked with red dots were deployed and centered around the trial well (blue star). Observe seven parallel lines running in the NS and EW directions with 25 m sampling along and between the lines.

[1]Saudi Aramco, EXPEC Advanced Research Center, Geophysics Technology, Dhahran, Saudi Arabia. E-mail: ali.dawood.18@aramco.com; emad.hemyari@aramco.com; ilya.silvestrov@aramco.com; a_bakulin@yahoo.com.

DOI:10.1190/tle40050374.1

check-shot profiles, ahead-of-the-bit predictions, and subsurface imaging at less cost than conventional wireline VSP acquisition. The system also saves rig time because conventional advanced borehole geophysics surveys (walkaway or 3D VSP) often take days to weeks for acquisition. Conventional acquisition also depends on the availability of vibroseis trucks and multilevel downhole tools and is subject to season- or weather-dependent source accessibility of the terrain.

SWD can be used to obtain an accurate subsurface reservoir structure by imaging the borehole data using Kirchhoff migration kernels (Bernasconi, 2002; Poletto and Miranda, 2004). Miranda et al. (2002) demonstrate how 3D SWD data could be migrated to better define reservoir geometry using 3D Kirchhoff migration. Poletto et al. (2003) show how 3D drill-bit imaging could be obtained during drilling and used to assist drilling and geologic interpretation. Rocca et al. (2005) test a 3D Kirchhoff migration algorithm in the frequency domain on synthetic and field SWD data, which provides images comparable to stacks from surface seismic reflection data. Kazemi et al. (2019) show how least-squares migration could be used to image SWD data and improve subsurface illumination as the downhole source gets closer to the target. As a result, it can deliver broader reflection-angle coverage of the target compared to surface seismic data.

Conventional borehole seismic acquisition does not often yield a reliable measurement of the wavefield in the shallow (0–1500 m) section due to multiple casing strings that are not perfectly cemented (Bakulin et al., 2020). SWD can reduce this gap significantly. Bakulin et al. (2020) demonstrate a reliable check shot up to a depth of 565 m with a top-drive pilot. Using a downhole pilot, check shots could be extended to 225 m below ground level, similar to deep seismic upholes. These results will be presented in a future publication. To summarize, SWD could enable accurate near-surface characterization of complex terrains, which is usually not possible using deep wells and requires additional uphole surveys. Poletto et al. (2003) show a reverse SWD VSP at an offset of 1242 m away from the well, which recorded accurate wavefields, illuminating reflectors at less than 1000 m deep. Rocca et al. (2005) show a common-source gather from a bit depth of approximately 469 m that shows relatively low S/N data due to the absorption of seismic energy in the shallow layers.

Ahead-of-the-bit prediction is critical to optimize drilling parameters and set casing and coring points. It is also crucial to identify hazards ahead of the bit, such as faults, overpressured zones, and formation variations (Greenberg, 2008). Miranda et al. (2002) demonstrate the utilization of 3D migration of reflection SWD wavefields to predict a geologic interface ahead of the bit. Poletto et al. (2003) use 3D imaging of SWD data to predict a critical hard quartz sandstone layer about 180 m ahead of the bit.

In this paper, we extracted two orthogonal 2D lines (east–west [EW] and north–south [NS]) from the first field trial data set. Each line delivers a separate reverse walkaway VSP (WAVSP). While both top-drive and downhole near-bit (memory) pilots were recorded, in this study, we utilize only the former to deconvolve the data, focusing on the assessment of real-time while-drilling imaging capability in a complex desert environment. We apply 2D migration to both WAVSP lines and evaluate the image of the overburden and the target reflectors ahead of the bit and away from the well. A specialized workflow is applied to the preprocessed SWD data to obtain high-quality reverse WAVSP data sets. The upgoing reflections in the shallow part are extracted and migrated using a 2D Kirchhoff migration algorithm. The results show the workflow's ability to enhance challenging low S/N SWD data from a weak drill-bit source and image a critical shallow reflector associated with a major change in the compressional wave velocity profile. The results also demonstrate the utilization of SWD data to image a key target horizon ahead of the bit.

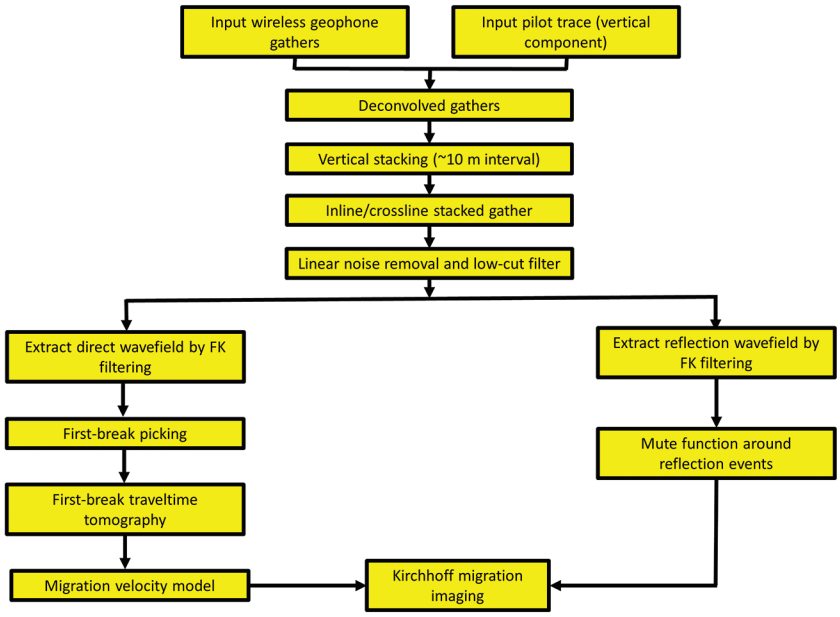

Figure 2. Complete processing workflow for obtaining enhanced SWD gathers and migrated images along the EW and NS reverse WAVSP lines.

Two-dimensional SWD processing

The EW WAVSP uses seven parallel receiver lines with 25 m inline and 25 m crossline spacing (Figure 1). They consist of 1250 receivers, representing 50% of the entire channel count. Likewise, the NS line also consists of seven lines with 1100 stations and similar spacing. The workflow used for the reconstruction of upgoing reflection events from SWD data along the two walkaway lines is shown in Figure 2. The processed upgoing drill-bit reflections were subsequently migrated to obtain a subsurface image.

The top-drive sensor's vertical component is used as a pilot estimation of the highly variable and complex drill-bit source signature. Vertical-component geophones are linked to wireless stations and time-synchronized with the

top-drive sensor. The recorded traces are deconvolved using the estimated pilot (Poletto et al., 2001). Each SWD trace is then obtained by stacking the recordings over a drilling interval of 32 ft (approximately 10 m), equivalent to one drill pipe length. The importance and details of this stacking process are explained by Poletto and Miranda (2004) and Bakulin et al. (2020). The workflow results in generating conventional common-source records with the shot position corresponding to the middle of the 32 ft stacked drilling interval. Typical land seismic data in the area are recorded with a minimum nine-geophone array and two vibrators. Conventional seismic data also require significant preprocessing due to low S/N caused by scattering in the complex near surface (Bakulin et al., 2019). SWD recordings with only a single sensor exhibit even lower S/N (Bakulin et al., 2020). To enhance the data quality in a manner similar to surface seismic, we apply an additional supergrouping (Bakulin et al., 2018) by stacking seven receiver lines in the crossline direction. Supergrouping applied to both NS and EW lines is an essential step of SWD preprocessing in a desert environment, as demonstrated by Bakulin et al. (2020), for less complicated check-shot applications.

Typical gathers enhanced by supergrouping along the EW and NS lines are shown in Figure 3. The direct and reflected arrivals caused by the drill bit are contaminated by intense surface noise from the drilling operations' vibrating equipment. Shale shakers, engines, and generators at the rig site are examples of surface sources that cause intense noise, as marked by the red arrows in Figure 3. This noise typically has a low dominant frequency compared with dill-bit reflections and direct arrivals. This surface-wave noise is also stationary compared to the drill-bit signal, which changes as the drill bit moves deeper (Poletto and Miranda, 2004). The low-frequency nature of the surface noise enables the suppression of the surface waves by a high-pass filtering sequence (Petronio et al., 1999; Wang et al., 2008). Figures 4a and 4b show corresponding gathers after low-cut filtering and linear noise removal in the common-shot domain. The suppression of the linear ground-roll energy is evident. Also, the elimination of surface noise with dominant frequencies below 20 Hz cleans up the records further. As a result, the direct and reflected arrivals caused by the drill bit are significantly enhanced.

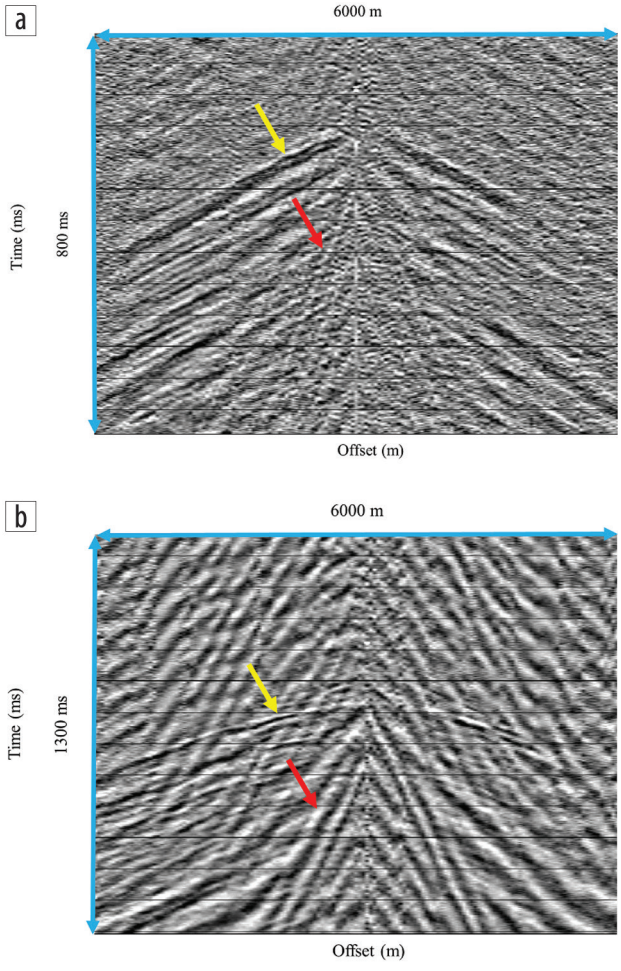

Figure 3. Typical enhanced common-shot gathers after supergrouping seven receiver lines: (a) EW line and (b) NS line. The EW line gather is acquired using a drill bit at a depth of 856 m, while the NS line gather is obtained when the drill bit was at a depth of 1838 m. The direct arrivals (yellow arrows) are clearly visible on both gathers. In contrast, reflection arrivals from the drill-bit source are still masked by the intense low-frequency groundroll energy (red arrows).

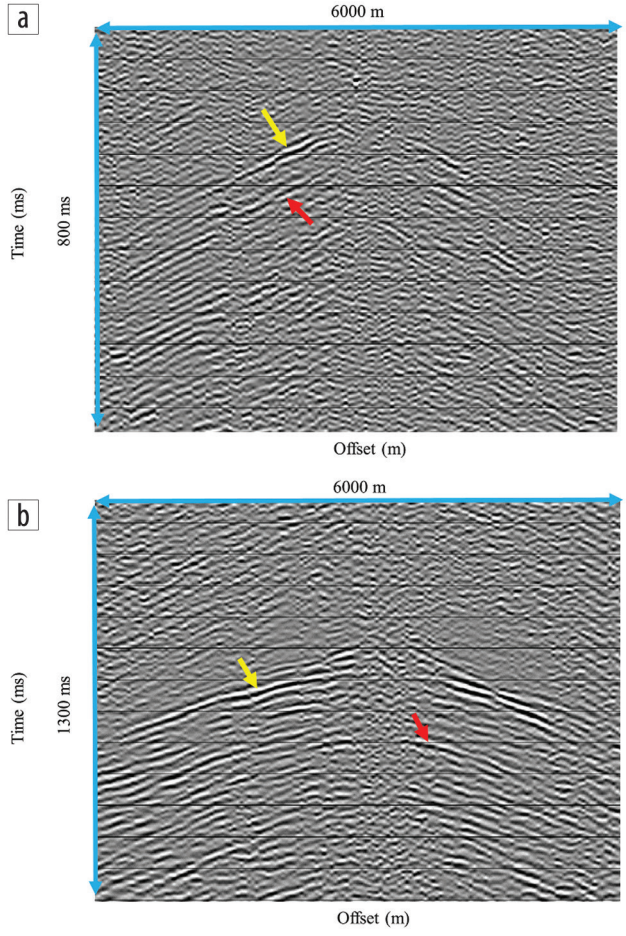

Figure 4. Same as Figure 3 but after additional linear noise removal and low-cut filtering: (a) EW reverse WAVSP line and (b) NS reverse WAVSP line. Linear noise removal suppresses various noises with lower apparent velocity, whereas low-cut filtering annihilates the dominant surface-wave noise with dominant frequencies below 20 Hz. The direct and reflection arrivals are enhanced and marked by yellow and red arrows, respectively.

The enhanced SWD gathers after low-cut filtering and linear noise removal were subsequently subjected to frequency-wavenumber (*f-k*) filtering to enhance the direct wavefield from the drill bit to the combined receiver stations. Figure 5 shows typical common-receiver gathers along the EW and NS lines after applying *f-k* filtering to enhance direct arrivals. These gathers were used for first-break picking, with picks fed into the traveltime tomographic inversion to update the velocity model around the well. Another run of *f-k* filtering was applied to the processed SWD gathers to extract and enhance upgoing reflection events along each line.

All gathers were subject to careful quality control, and only higher-quality data were selected for migration. While separate migration of gathers with lower prestack S/N (and migration of the entire data) was attempted, the resulting image was not consistent with logging or surface seismic data sets. These findings are consistent with 2D seismic data, which often experience wipeout zones (Rensbergen et al., 2003) in the areas affected by near-surface complexities. Such wipeouts can only be fixed by acquiring and processing 3D seismic, covering all possible azimuths, including those undershooting near-surface anomalies. In the Middle East, the abundance of such shallow anomalies can damage and defocus even 3D seismic images, as Reilly et al. (2010) show. In the absence of 3D coverage, we decided to proceed with the 2D migration of selected gathers with higher prestack S/N.

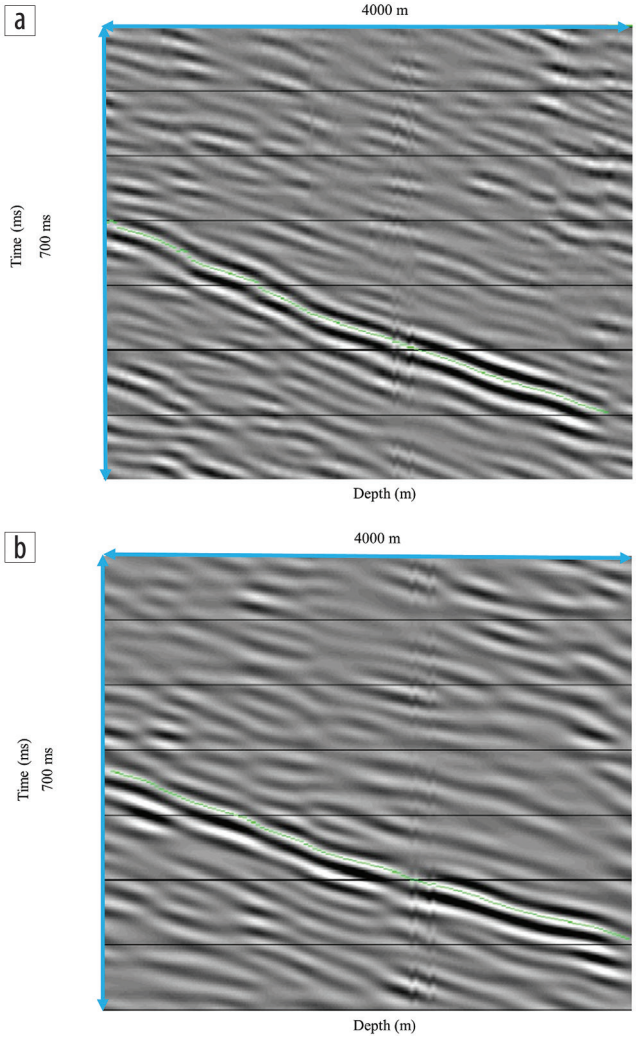

Figure 5. Typical VSP common-receiver gathers after *f-k* filtering to enhance direct arrivals: (a) EW line and (b) NS line. The green dots denote the first-break picks that are subsequently used for traveltime tomographic inversion.

Along the EW direction, we extracted high-quality shallow upgoing reflection events from 36 receiver stations and drill-bit depths covering an interval approximately from 650 to 1850 m. Three representative receiver gathers are plotted in Figure 6, showing strong prestack reflection events at about 1 km depth (marked by black arrows). These reflected events are associated with a boundary with significant acoustic impedance contrast. Likewise, for the NS direction, 45 receiver stations showed quality ahead-of-the-bit upgoing reflections from target layers with drill-bit depths from 600 to 1900 m. These reflection events are associated with a target zone at a depth of about 2 km, and they are marked in Figure 7 by black arrows on three representative receiver gathers. Note, that the same strong shallow boundary at approximately 1 km in the EW gathers gives rise to strong PS-mode conversions, indicated by dashed arrows on the gathers before wavefield separation (Figure 7).

Two-dimensional SWD imaging

Now that we have derived the velocity model around the well and preconditioned the data, such that it consists predominantly of upgoing reflections, the goal is to obtain subsurface images along the NS and EW WAVSP lines. The following Kirchhoff migration operator (Claerbout, 1992) was used to image the upgoing reflections extracted from the SWD gathers:

$$m(x) = \int_{s,g,\omega} d(s,g,\omega)\, e^{-i\omega\left(\tau_{sx}+\tau_{xg}\right)}\, ds\, dg\, d\omega\,, \qquad (1)$$

where $m(x)$ is the migrated image representing the subsurface structure, $d(s,g,\omega)$ is the seismic reflection data recorded by the wireless surface receiver g caused by the drill-bit source s at the current depth, and ω is the angular frequency. τ_{sx} is the computed traveltime from the source at the current depth position s to the subsurface trial reflection point x. Similarly, τ_{xg} is the computed traveltime from the subsurface trial image point x to the wireless surface receiver g. These traveltimes are computed using the migration velocity model obtained from the first-break traveltime tomographic inversion. The Kirchhoff migration is the most favorable method to migrate VSP and SWD data sets because the data sets have much smaller volumes than surface seismic data (Bicquart, 1988; Dillon, 1988).

While the velocity model was updated using picks from all available shot gathers, the migrated image was obtained by migrating only 36 receivers west of the well (marked by the red stars in Figure 8a). These receivers captured the reflection events from shallow layers. A narrow mute function is applied around the upgoing reflections to obtain an enhanced image of these layers. A check-shot profile extracted from the nearest usable offset

receiver to the wellhead, representing an inverse zero-offset VSP (ZVSP) gather, is shown in Figure 9a. The arrow in the figure marks the depth of a major acoustic impedance contrast due to the presence of a highly porous carbonate layer overlaid by compacted clastic layers, which yields a high slope change in the time-depth curve as shown in Figure 9b. The EW-migrated section is plotted in Figure 9c and overlaid by the compressional wave delay time and shear-wave delay time sonic logs in blue and brown, respectively. These logs are borrowed from a nearby fully logged well, including the shallow section. The logs superimposed on the migrated depth image clearly show the strongest reflector's agreement with a high-contrast boundary seen on the logs. Identifying this contrasting overburden layer is critical for geologists and drillers. It usually corresponds to a lost-circulation zone with a fast penetration rate, requiring the adjustment of mud-weight parameters and setting an accurate casing point.

The velocity model overlaid by the Kirchhoff-migrated image along the NS reverse WAVSP line is shown in Figure 8b. The velocity model is updated using traveltime tomography with all available picks. In contrast, the migrated section is obtained by imaging upgoing reflection events from only 45 receivers north of the well (marked by red stars). These upgoing reflections are ahead of the current bit location, and the Kirchhoff migration helped to accurately position them ahead of the bit. The imaged layers are at a depth of approximately 2 km. They are associated with a major impedance contrast due to a formation change from thick and compacted anhydrite to underlying porous and soft carbonate layers. This target image helps interpreters update the respective formation tops ahead of the current bit depth. After conversion to time, an extracted narrow SWD image near the well (Figure 10) has a good tie with the NS-migrated section from surface seismic, showing the continuous target layer. After applying the correlation shift to match the two data sets, the interpreter updated their

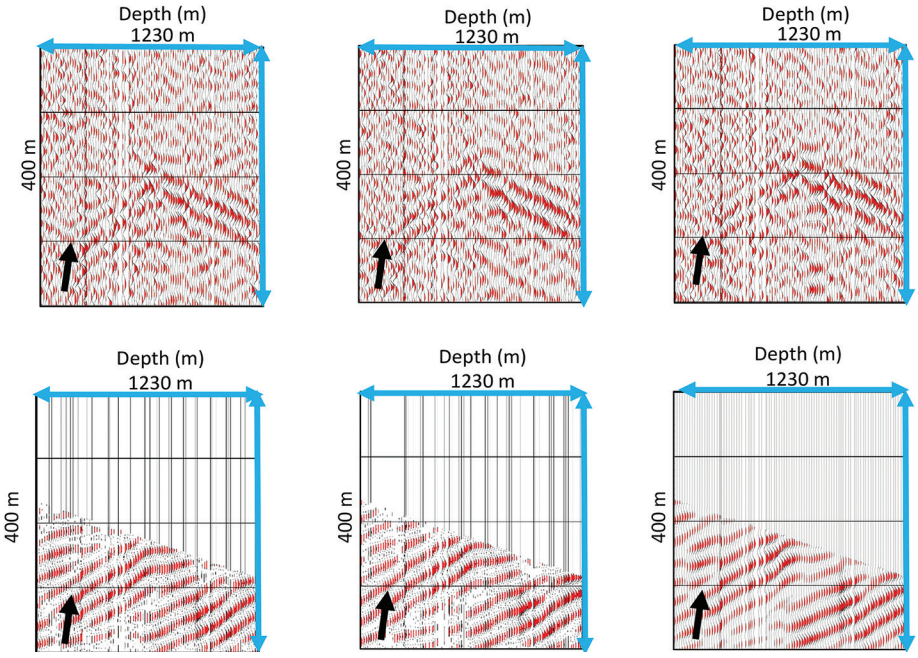

Figure 6. Three common-receiver gathers before (top) and after (bottom) enhancing upgoing reflection events along the EW reverse WAVSP line. The reflection events, marked with black arrows, are associated with a significant change in acoustic impedance at approximately 1 km depth.

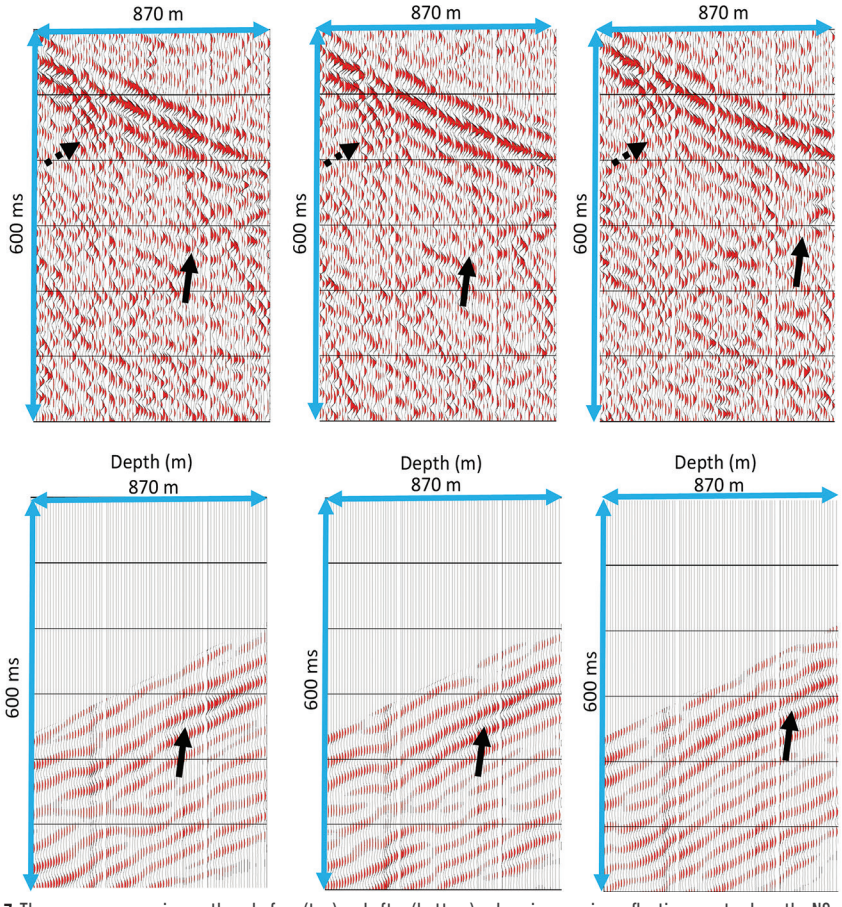

Figure 7. Three common-receiver gathers before (top) and after (bottom) enhancing upgoing reflection events along the NS reverse WAVSP line. The reflection events, marked with black arrows, are associated with the target horizon at about 2 km depth. The dashed arrows denote the mode-converted energy occurring at the contrasting boundary at approximately 1 km.

predicted formation top for this layer to be 15 m higher than the surface seismic prognosed depth. The newly updated horizon's depth was confirmed postdrilling by analyzing the drill cutting samples in the field.

The two images demonstrate SWD's ability to provide accurate subsurface images around and ahead of the bit, thus achieving a primary objective of any SWD system — acquiring borehole seismic data and enabling optimal drilling decisions in real time without incurring additional rig time and avoiding well intervention.

Conclusions

We presented an imaging case study that utilizes data from an onshore SWD system to image around and ahead of the bit. Only a surface top-drive pilot was used in this study to evaluate the quality of the imaging that could be achieved in real time. Two orthogonal reverse WAVSP receiver lines were extracted from the SWD trial's multiazimuth 3D acquisition geometry in a desert environment. A specialized workflow was applied to enhance the challenging single-sensor data extracted along the EW and NS directions with the low S/N caused by a weak source and complex near surface. The flow aims to deconvolve the drill-bit source signature, suppress the rig noise, and increase the S/N of the weaker reflections generated by the drill-bit source. Similar to surface seismic with active sources, supergrouping of seven receiver lines was particularly useful in drastically improving the S/N and boosting weak reflected signals. Low-cut frequency and *f-k* filtering steps in the common-receiver domain effectively enhanced the direct wavefield and upgoing reflection events along WAVSP lines. The enhanced direct wavefields were used to pick first-arrival traveltimes utilized by traveltime tomography delivering robust migration velocity models. These velocity models (one for each orthogonal plane) were subsequently used to migrate the enhanced upgoing reflection events from the two walkaway lines.

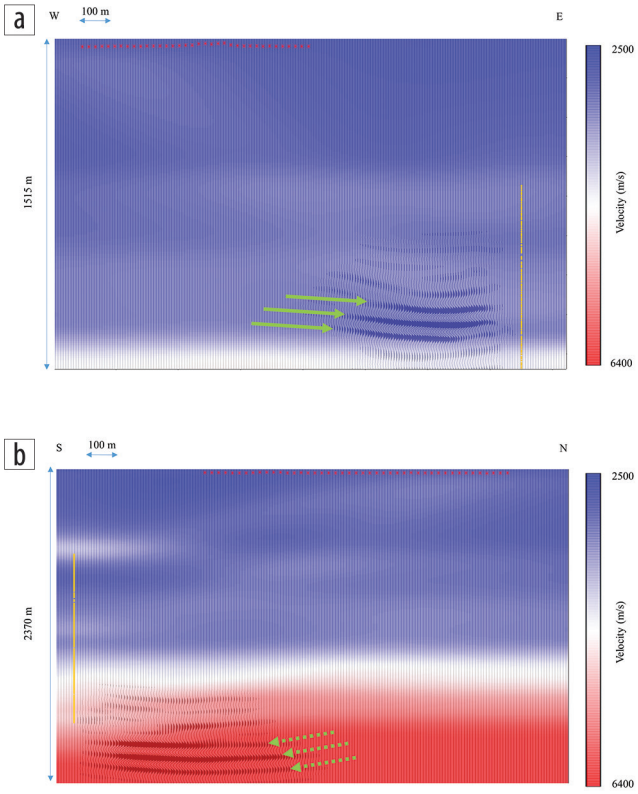

Figure 8. The migration velocity model overlaid by the Kirchhoff-migrated images: (a) EW line and (b) NS line. Solid green arrows denote strong overburden reflectors at about 1 km depth imaged west of the well. Dashed green arrows identify deeper ahead-of-the-bit target horizons at about 2 km, which are imaged up to 600 m north of the well. The red stars denote surface receivers used for imaging. Likewise, the yellow squares denote the drill-bit source locations used for migration.

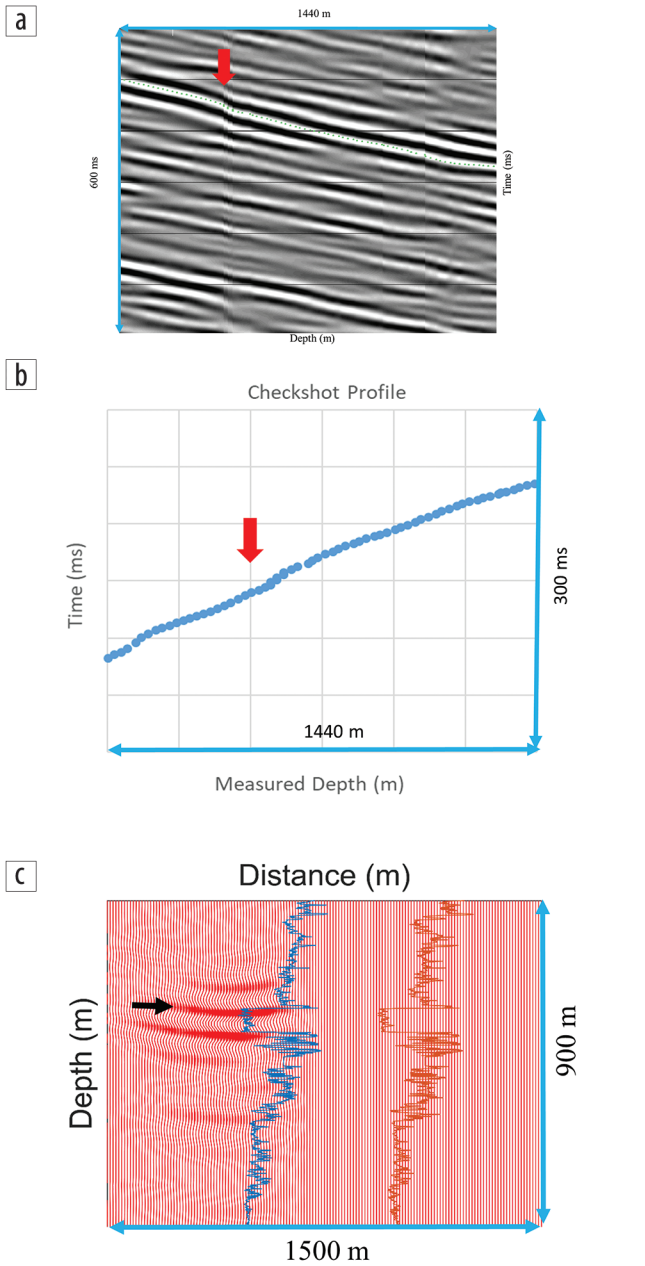

Figure 9. ZVSP gather of the (a) direct wave and (b) extracted check-shot profile confirms the existence of a boundary with a significant change in acoustic impedance marked by the red arrows. This boundary gives rise to the strong reflector marked by the black arrow on the (c) EW-migrated section. (c) This migrated image is further superimposed with sonic logs (compressional and shear) from a nearby well, validating excellent alignment in the depth of the imaged overburden reflector and the highly contrasting regional marker on acoustic logs.

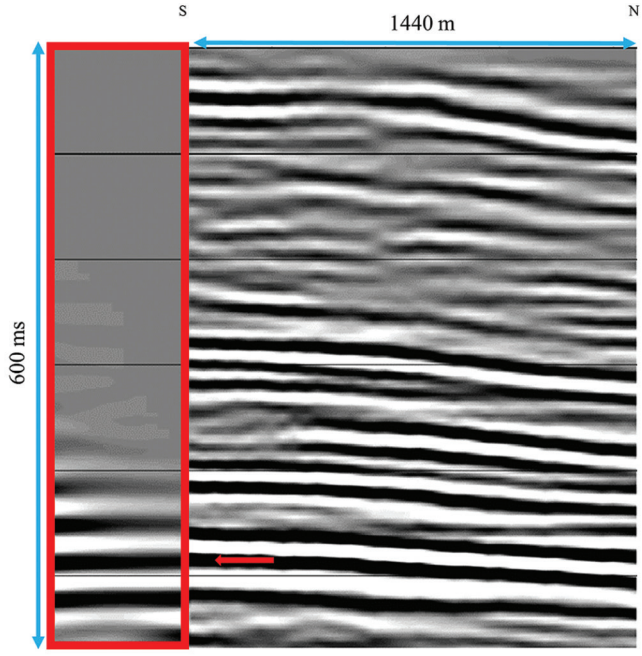

Figure 10. The red rectangle outlines a narrow SWD migrated image near the well (similar to Figure 8b but converted to time). SWD image ties remarkably with the NS-migrated section obtained from surface seismic. The red arrow marks a key target horizon.

To obtain cleaner migrated sections, mute functions were applied to exclude low S/N data caused by complex near surface.

The EW reverse WAVSP successfully imaged the shallower portion of the overburden around the bit. The migrated image delineated a strong regional reflector associated with a significant change in lithology and acoustic impedance at approximately 1 km depth. The NS line imaged a deeper subsurface horizon ahead of the bit and away from the well. This WAVSP image of a target reflector at approximately 2 km depth matches the migrated surface seismic section excellently. The presented imaging can be conducted in real time because wireless geophones and top-drive sensors transmit continuous data immediately available for processing. This case study validates the SWD system's real-time capability to image around and ahead of the bit. The SWD system helps geologists and drillers make optimal drilling decisions and avoid geohazards while delivering reliable borehole seismic data for well ties and seismic calibration without using extra rig time or invoking well intervention. TLE

Acknowledgments

We thank Mustafa Al-Ali and Abdulaziz Al-Muhaidib (Saudi Aramco) for initiation and advancement of the DrillCAM project. We are grateful to Hussein Rashad Abdelghani, Bilal Tariq, and Peter Ezi (Saudi Aramco Gas Drilling) for supporting the field trial. We thank Flavio Poletto, Piero Corubolo, Andrea Schleifer, Fabio Meneghini, Franco Zgauc, and Biancamaria Farina (Istituto Nazionale di Oceanografia e di Geofisica Sperimentale) for their technical support.

Data and materials availability

Data associated with this research are confidential and cannot be released.

Corresponding author: ali.dawood.18@aramco.com

References

Al-Muhaidib, A., Y. Liu, P. Golikov, E. Al-Hemyari, Y. Luo, and M. Al-Ali, 2018, DrillCAM: A fully integrated real-time system to image and predict ahead and around the bit: 88th Annual International Meeting, SEG, Expanded Abstracts, 719–723, https://doi.org/10.1190/segam2018-2995323.1.

Bakulin, A., P. Golikov, M. Dmitriev, D. Neklyudov, P. Leger, and V. Dolgov, 2018, Application of supergrouping to enhance 3D prestack seismic data from a desert environment: The Leading Edge, **37**, no. 3, 200–207, https://doi.org/10.1190/tle37030200.1.

Bakulin, A., I. Silvestrov, and D. Neklyudov, 2019, Where are the reflections in single-sensor land data?: Presented at the SEG Workshop on New Advances in Seismic Land Data Acquisition.

Bakulin, A., A. Aldawood, I. Silvestrov, E. Hemyari, and F. Poletto, 2020, Seismic-while-drilling applications from the first DrillCAM trial with wireless geophones and instrumented top drive: The Leading Edge, **39**, no. 6, 422–429, https://doi.org/10.1190/tle39060422.1.

Bernasconi, G., 2002, Kirchhoff depth migration of 3D SWD data: 64th Conference and Exhibition, EAGE, Extended Abstracts, https://doi.org/10.3997/2214-4609-pdb.5.P012.

Bertelli, L., and F. di Cesare, 1999, Improving the subsurface geological model while drilling: First Break, **17**, no. 6, https://doi.org/10.1046/j.1365-2397.1999.00706.x.

Bicquart, P., 1998, Application of Kirchhoff depth migration to 3D-VSP: 68th Annual International Meeting, SEG, Expanded Abstracts, 389–392, https://doi.org/10.1190/1.1820443.

Claerbout, J. F., 1992, Earth surroundings analysis: Processing versus inversion: Blackwell Scientific Publications.

Dillon, P., 1988, Vertical seismic profile migration using the Kirchhoff integral: Geophysics, **53**, no. 6, 786–799, https://doi.org/10.1190/1.1442514.

Greenberg, J., 2008, Seismic while drilling keeps bit turning to right while acquiring key real-time data: Drilling Contractor, **64**, no. 2, 44–45.

Haldorsen, J. B., D. E. Miller, and J. J. Walsh, 1995, Walk-away VSP using drill noise as a source: Geophysics, **60**, no. 4, 978–997, https://doi.org/10.1190/1.1443863.

Kazemi, N., D. Trad, K. Innanen, and R. Shor, 2019, Joint least-squares RTM of surface seismic and seismic-while-drilling datasets: 81st Conference and Exhibition, EAGE, Extended Abstracts, https://doi.org/10.3997/2214-4609.201900697.

Khaled O. S., A. M. Al-Ateeqi, A. R. James, and R. J. Meehan, 1996, Seismic-while-drilling in Kuwait: Results and applications: GeoArabia, **1**, no. 4, 531–550.

Mathiszik, H., M. Cox, F. Bøen, S. Petersen, A. Sæbø, and R. Coman, 2011, Seismic while drilling in the Grane Field: 1st Workshop on Borehole Geophysics, EAGE, https://doi.org/10.3997/2214-4609.20145267.

Miranda, F., L. Aleotti, F. Abramo, F. Poletto, A. Craglietto, S. Persoglia, and F. Rocca, 1996, Impact of the seismic while drilling technique on exploration wells: First Break, **14**, no. 2, https://doi.org/10.3997/1365-2397.1996004.

Miranda, F., F. Poletto, L. Bertelli, L. Petronio, and B. Gressetvold, 2002, A SWD 3D RVSP onshore survey — Imaging and final results: 64th Conference and Exhibition, EAGE, Extended Abstracts, https://doi.org/10.3997/2214-4609-pdb.5.P015.

Petronio, L., F. Poletto, F. Miranda, and G. Dordolo, 1999, Optimization of receiver pattern in seismic-while-drilling: 69th Annual International Meeting, SEG, Expanded Abstracts, 164–167, https://doi.org/10.1190/1.1820847.

Poletto, F., and F. Miranda, 2004, Seismic while drilling: Fundamentals of drill-bit seismic for exploration: Elsevier.

Poletto, F., M. Malusa, and F. Miranda, 2001, Numerical modeling and interpretation of drillstring waves: Geophysics, **66**, no. 5, 1569–1581, https://doi.org/10.1190/1.1487102.

Poletto, F., L. Petronio, F. Miranda, M. Malusa, A. Schleifer, P. Corubolo, C. Bellezza, R. Miandro, and B. Gressetvold, 2003, Prediction and 3D imaging while drilling by drill-bit 3D RVSP: 65th Conference and Exhibition, EAGE, Extended Abstracts, https://doi.org/10.3997/2214-4609-pdb.6.P221.

Rector, J. W., and B. P. Marion, 1991, The use of drill-bit energy as a downhole seismic source: Geophysics, **56**, no. 5, 628–634, https://doi.org/10.1190/1.1443079.

Reilly, J. M., A. P. Shatilo, and Z. J. Shevchek, 2010, The case for separate sensor processing: Meeting the imaging challenge in a producing carbonate field in the Middle East: The Leading Edge, **29**, no. 10, 1240–1249, https://doi.org/10.1190/1.3496914.

Rensbergen, P., R. Hillis, A. Maltman, and C. Morley, 2003, Subsurface sediment mobilization: Geological Society of London.

Rocca, F., M. Vassallo, and G. Bernasconi, 2005, Three-dimensional seismic-while-drilling (SWD) migration in the angular frequency domain: Geophysics, **70**, no. 6, S111–S120, https://doi.org/10.1190/1.2106050.

Wang, L., H. Liu, S. Tong, and M. Wei, 2008, Extracting the weak signal of the drill-bit from seismic while drilling data: International Workshop on Education Technology and Training and International Workshop on Geoscience and Remote Sensing, IEEE, https://doi.org/10.1109/ETTandGRS.2008.86.